

## Target Fragmentation in Oxygen-Emulsion Collisions at Dubna and SPS Energies

Fu-Hu Liu<sup>□</sup>

*Institute of Modern Physics and Department of Physics, Shanxi Teachers University,  
Linfen, Shanxi 041004, China*

(Received August 16, 2001)

The experimental results of target fragmentation in oxygen-emulsion collisions at the Dubna energy (a few A GeV) and the Super Proton Synchrotron (SPS) energy (60-200A GeV) are reported. The multiplicity distributions of target fragments, the correlations between the multiplicity distributions and the projectile fragments, as well as the correlations between the black and grey fragments are given.

PACS. 25.75.-q – Relativistic heavy ion collisions.

PACS. 25.70.Mn – Projectile and target fragmentation.

PACS. 25.70.Pq – Multifragment emission and correlations.

### I. Introduction

According to the “participant-spectator model” [1], the interacting system in relativistic nucleus-nucleus collisions can be divided into three parts: a target spectator, a participant, and a projectile spectator. The overlapping part of the two colliding nuclei is called the participant and the other parts are called the target spectator and the projectile spectator, respectively. The velocity of the participant has a wide distribution from zero to the projectile velocity. The velocity of the target spectator in the laboratory reference frame is almost zero. The projectile spectator has almost the same velocity as that of the projectile. It is known that violent collisions happen in the participant, and weak excitations and cascade collisions happen in the spectator. The participant produces many mesons, nucleons, photons, and lepton pairs, etc., and the spectator fragments into many nucleons and nuclei.

There are relations between the participant and the spectator. It is expected that a quark-gluon plasma (quark matter) will be formed in the participant at very high incident energies, and a liquid-gas phase transition will happen in the spectator. Both the participant and the spectator are relevant for studying the nuclear reaction mechanism. For the purpose of studying the nuclear reaction mechanism, it is highly important to investigate the spectator fragmentation.

The Dubna energy is a special energy, at which the nuclear limiting fragmentation applies initially. For oxygen the limiting fragmentation may set in at or below the Dubna energy. At present the highest energy for studying nucleus-nucleus collisions by a fixed target is the Super Proton Synchrotron (SPS) energy. To study nuclear fragmentation, e.g., oxygen induced nuclear fragmentation at the Dubna energy and at the SPS energy, is of great importance.

The characteristics of the nuclear spectator fragmentation can be described by the multiplicity, angular, mass, and charge distributions and the correlations. The aim of the present work is to perform a systematic analysis of target fragmentation in oxygen-emulsion collisions at

3.7A GeV (the Dubna energy) and at 200A GeV (the SPS energy). The second section describes the experimental materials. The experimental multiplicity distributions of target fragments, the correlations between the multiplicity distributions and the projectile fragments, as well as the correlations between the black and grey fragments are given in the third, fourth, and fifth sections, respectively. The last section gives our conclusion.

## II. Experimental materials

The nuclear emulsion stacks measured in the experiment were exposed by the oxygen beams at the Synchrophasotron of the Joint Institute for Nuclear Research (JINR), Dubna, Russia and at the SPS of the European Organization for Nuclear Research (CERN), Geneva, Switzerland, respectively. The beam energies are 3.7A and 200A GeV, respectively. The emulsion type is Russian NIKFI-BR2 and the pellicle size is 10 cm  $\times$  10 cm  $\times$  600  $\mu$ m.

Each interaction was scanned using the “along-the-track” method with the help of a Russian microscope of the Mbu9 type. We have excluded the events occurring within a 20  $\mu$ m thickness from the top or bottom surface of the pellicle. Great care has been taken in the identification of different tracks [2].

Three interaction types are found in the experiment. They are elastic collisions, electromagnetic dissociations, and nuclear reactions. An elastic collision is an interaction occurring between the projectile oxygen and the target hydrogen in the emulsion. The final state products are only the projectile oxygen and the target hydrogen. An electromagnetic dissociation is an interaction occurring between the projectile and the target due to electromagnetic interactions. The final state products contain the projectile fragments and/or the target fragments. A nuclear reaction is an interaction occurring between the two colliding nuclei due to nuclear interactions. The final state products contain the projectile fragments, the target fragments, the relativistic produced particles, and a few slow mesons.

We focus our attention on the nuclear reaction in the present work. The data studied in the present work consist of 266 random nuclear reaction events at 3.7A GeV and 446 random nuclear reaction events at 200A GeV.

## III. Multiplicity distribution of target fragments

The number of final state target fragments in an event is called the multiplicity of target fragments and denoted by  $N_h$ . The track grain density of target fragments in a nuclear emulsion is greater than  $1.4I_0$  [2, 3], where  $I_0$  denotes the experimental minimum value of the track grain density of a relativistic singly charged particle. We can divide target fragments into two parts: target black fragments and target grey fragments. The multiplicities of black and grey fragments are denoted by  $N_b$  and  $N_g$ , respectively. The residual range of black fragments is less than or equal to 3 mm, and that of grey fragments is greater than 3 mm. For a proton, the kinetic energy corresponding to a residual range of 3 mm is 26 MeV [3]. We can measure the track grain densities and residual ranges of all the target fragments. Then, the multiplicity distribution of each kind of target fragment can be obtained.

Figure 1 presents the multiplicity distributions of target fragments produced in oxygen-emulsion collisions at 3.7A GeV (dotted histograms) and 200A GeV (solid histograms), respectively. Figures 1(a), 1(b), and 1(c) correspond to  $N_b$ ,  $N_g$ , and  $N_h$  distributions, respectively.

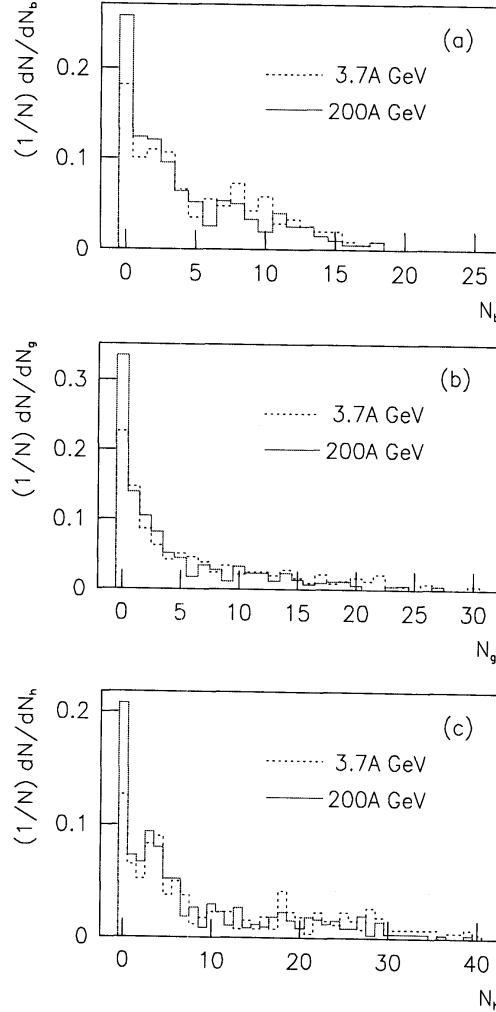


FIG. 1. Multiplicity distributions of target fragments produced in oxygen-emulsion collisions at 3.7A GeV (dotted histograms) and 200A GeV (solid histograms). The  $N_b$ ,  $N_g$ , and  $N_h$  distributions correspond to Figs. 1(a), 1(b), and 1(c), respectively.

One can see that the multiplicity distributions of target fragments in oxygen-emulsion collisions at the two different energies are similar. The differences are mainly in the probabilities of events with  $N_i = 0$  ( $i = b, g, \text{ and } h$ ) and the distribution region of  $N_g$ .

Table I presents the mean multiplicity,  $\langle N_i \rangle$ , of target fragments produced in oxygen-emulsion collisions at 3.7A GeV (upper panel) and 200A GeV (lower panel), respectively. The emulsion nuclei are divided into two parts: the light nuclei (C/N/O,  $N_h \cdot 8$ ) and the heavy nuclei (Ag/Br,  $N_h > 8$ ). One can see that the values of  $\langle N_i \rangle$  at 3.7A GeV are greater than those at 200A GeV. The differences for light nuclei are smaller than those for heavy nuclei. The differences between the values of  $\langle N_b \rangle$  are smaller than those of  $\langle N_g \rangle$ .

TABLE I. Mean multiplicities of target fragments in oxygen-emulsion collisions at 3.7A GeV (upper panel) and 200A GeV (lower panel). Events are divided into three parts: C/N/O, emulsion, and Ag/Br.

Target ( $N_h$ region)	$\langle N_b \rangle$	$\langle N_g \rangle$	$\langle N_h \rangle$
C/N/O ( $N_h \leq 8$ )	1.6 $\pm$ 0.1	1.3 $\pm$ 0.1	2.9 $\pm$ 0.2
Emulsion ( $N_h \leq 0$ )	5.1 $\pm$ 0.3	6.4 $\pm$ 0.5	11.5 $\pm$ 0.7
Ag/Br ( $N_h > 8$ )	9.5 $\pm$ 0.3	12.6 $\pm$ 0.7	22.1 $\pm$ 0.8
C/N/O ( $N_h \leq 8$ )	1.5 $\pm$ 0.1	1.1 $\pm$ 0.1	2.6 $\pm$ 0.1
Emulsion ( $N_h \leq 0$ )	4.1 $\pm$ 0.2	3.9 $\pm$ 0.2	8.0 $\pm$ 0.4
Ag/Br ( $N_h > 8$ )	9.3 $\pm$ 0.3	9.6 $\pm$ 0.4	18.9 $\pm$ 0.6

We can explain qualitatively the similarities and differences between the two different energies. (i) At the two energies, the incident nuclei are the same, and the target nuclei are the same, too. At the present accelerator energy region, the production of target fragments is mainly determined by the nuclear geometry. (ii) The impact parameter increases with the increase of the effect of the electromagnetic interaction between the projectile and target. This means an increase in the probability of events with low multiplicity. (iii) The target nucleus has a stopping power. The incident oxygen at 3.7A GeV can penetrate through the light nucleus and cannot penetrate through the heavy nucleus. But the incident oxygen at 200A GeV can penetrate through both the light and heavy nuclei. (iv) Target black fragments are mainly produced by the excitation of the target spectator. The excitation energies obtained by targets at the two incident energies are almost the same. This means that the difference between the  $\langle N_b \rangle$  are small. Target grey fragments are mainly produced by the cascade collisions in the target spectator and participant. The contribution of the target spectator is greater than that of the target participant. At low energy, the participant contribution decreases and the spectator contribution increases due to the target stopping effect. This means that the events with high  $N_g$  have a greater probability to appear.

#### IV. Correlations between multiplicity distributions and projectile fragments

In a nuclear emulsion, the charges of the projectile fragments can be measured by the grain density and  $\pm$ -ray counting methods [4], as well as the lacunarity measurement technique [5]. The track grain densities of projectile hydrogen and helium fragments are  $l_0$  and  $4l_0$ , respectively. For projectile fragments with charge  $Z > 2$ , we have used the  $\pm$ -ray counting method due to a very large track grain density. Let  $n_O$  and  $n_Z$  denote the experimental track  $\pm$ -ray densities of the incident oxygen nucleus and projectile fragment with charge  $Z$ , respectively. We have  $Z = 8 \frac{n_Z}{n_O}$ , where 8 is the charge of the oxygen nucleus. In nuclear emulsion, we can measure the charges of all the projectile fragments.

Let  $Q$  denote the bound system charge [6-8]. For the fragments with  $Z \geq 2$ , we have  $Q = \sum Z$  ( $Z \geq 2$ ). Because  $N_b$ ,  $N_g$ , and  $N_h$  are related to the impact parameter,  $Q$  is also a measurement of the impact parameter. The relationship between  $N_i$  and  $Q$  should be observed.

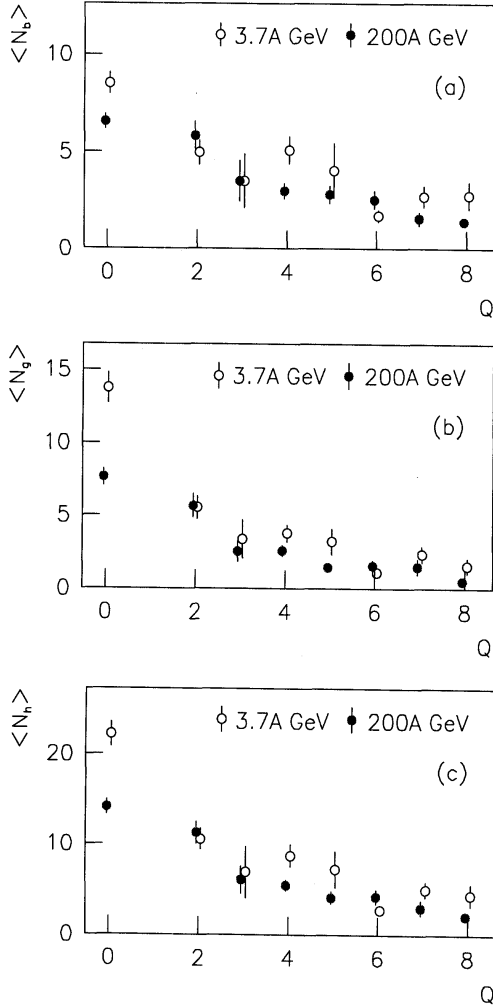


FIG. 2. Correlations between the target fragment multiplicities and the bound system charge in oxygen-emulsion collisions at 3.7A GeV (open circles) and 200A GeV (solid circles). Correlations of  $\langle N_b \rangle$  vs  $Q$ ,  $\langle N_g \rangle$  vs  $Q$ , and  $\langle N_h \rangle$  vs  $Q$  correspond to Figs. 2(a), 2(b), and 2(c), respectively.

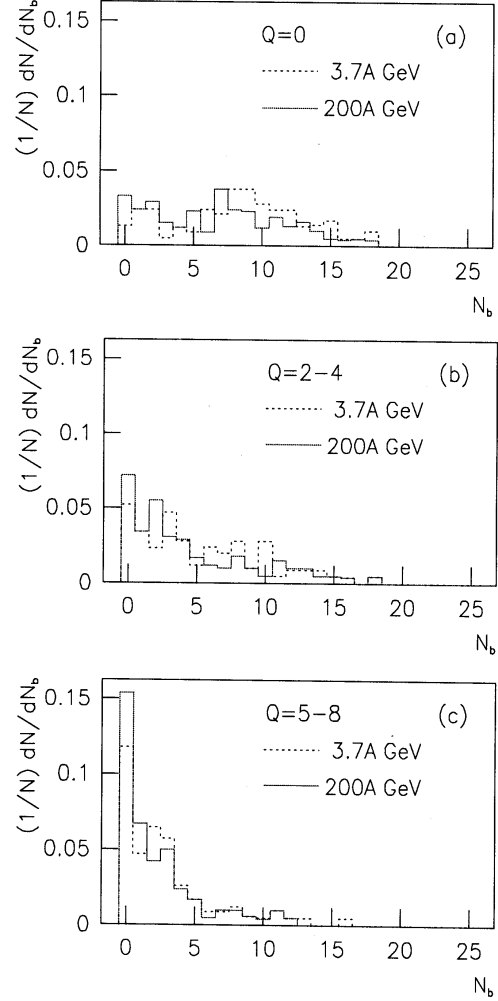


FIG. 3. The  $N_b$  distributions for events with different  $Q$  values in oxygen-emulsion collisions at 3.7A GeV (dotted histograms) and 200A GeV (solid histograms). The  $N_b$  distributions for  $Q = 0$ ,  $Q = 2$ – $4$ , and  $Q = 5$ – $8$  correspond to Figs. 3(a), 3(b), and 3(c), respectively.

Figure 2 gives the correlations between  $N_i$  and  $Q$  for oxygen-emulsion collisions at 3.7A GeV (open circles) and 200A GeV (solid circles), respectively. Figures 2(a), 2(b), and 2(c) correspond to the correlations of  $\langle N_b \rangle$  vs  $Q$ ,  $\langle N_g \rangle$  vs  $Q$ , and  $\langle N_h \rangle$  vs  $Q$ , respectively. One can see that negative correlations between  $\langle N_i \rangle$  and  $Q$  are obtained.

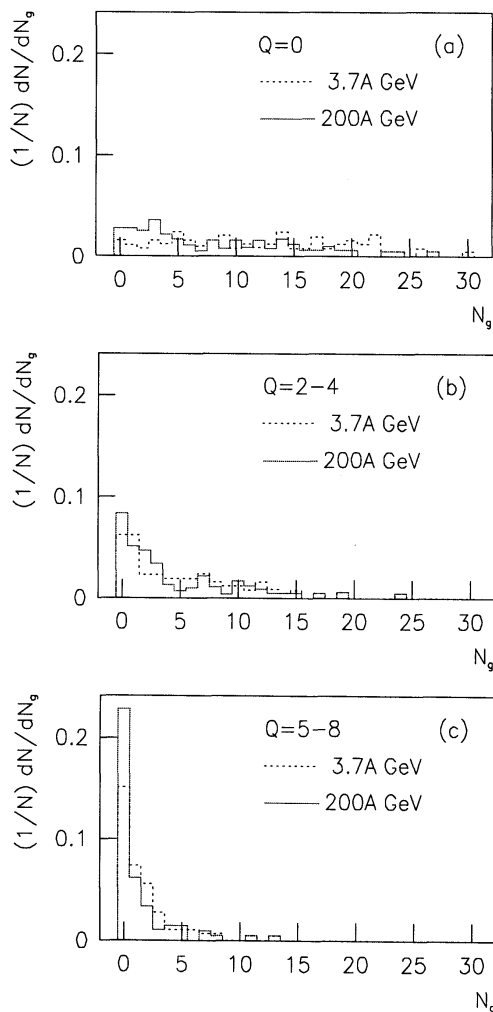


FIG. 4. As for Fig. 3, but showing the results of  $N_g$  distributions.

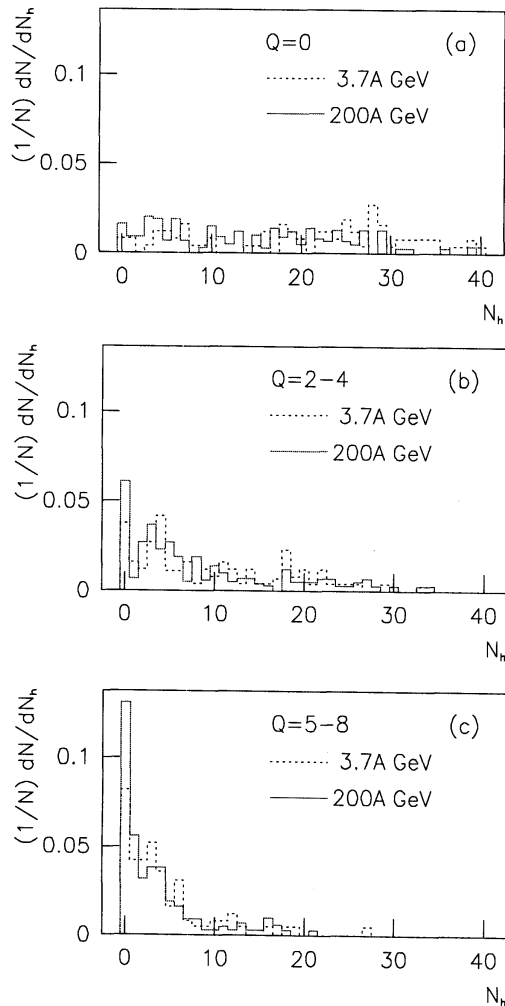


FIG. 5. As for Fig. 3, but showing the results of  $N_h$  distributions.

The  $N_b$ ,  $N_g$ , and  $N_h$  distributions for events with different  $Q$  regions are given in Figs. 3, 4, and 5, respectively. The dotted and solid histograms correspond to the experimental data of oxygen-emulsion collisions at 3.7A GeV and 200A GeV, respectively. Figures (a), (b), and (c) are the results for events with  $Q = 0$ ,  $Q = 2 ; 4$ , and  $Q = 5 ; 8$ , respectively. One can see that the multiplicity of target fragments has a wide and even distribution at small  $Q$ . The number of events with low multiplicity increases and the number of events with high multiplicity decreases with increasing value of  $Q$ . The multiplicity distribution becomes narrow at great  $Q$ .

The mean multiplicities of events with different  $Q$  are given in Table II. The upper and lower panels correspond to oxygen-emulsion collisions at 3.7A and 200A GeV, respectively. One can see that the mean multiplicities decrease with increasing value of  $Q$ .

TABLE II. Mean multiplicities of target fragments in oxygen-emulsion collisions at 3.7A GeV (upper panel) and 200A GeV (lower panel). Events are divided into three parts:  $Q = 0$ ,  $Q = 2-4$ , and  $Q = 5-8$ .

Q region	$\langle N_b \rangle$	$\langle N_g \rangle$	$\langle N_h \rangle$
Q = 0	8.5 § 0.6	13.6 § 1.0	22.1 § 1.3
Q = 2-4	4.9 § 0.4	4.6 § 0.5	9.4 § 0.8
Q = 5-8	2.4 § 0.3	1.6 § 0.2	4.0 § 0.5
Q = 0	6.5 § 0.4	7.5 § 0.6	14.0 § 0.9
Q = 2-4	4.3 § 0.4	3.9 § 0.4	8.2 § 0.7
Q = 5-8	2.1 § 0.2	1.2 § 0.2	3.3 § 0.3

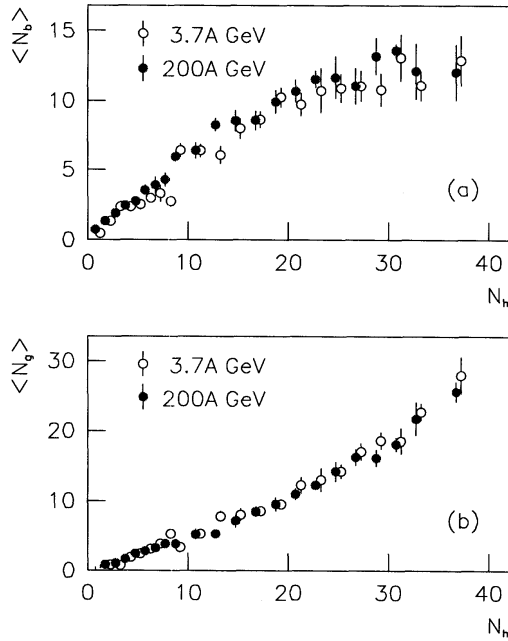


FIG. 6. Correlations between  $\langle N_b \rangle$  and  $N_h$  (a), as well as  $\langle N_g \rangle$  and  $N_h$  (b), in oxygen-emulsion collisions at 3.7A GeV (open circles) and 200A GeV (solid circles).

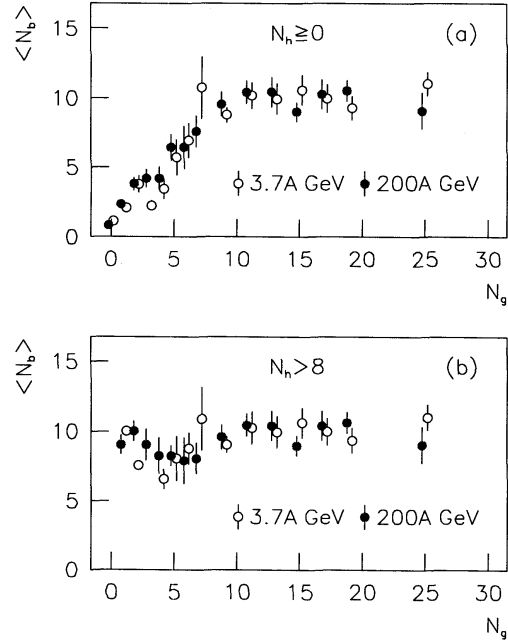


FIG. 7. Correlations between  $\langle N_b \rangle$  and  $N_g$  for events with  $N_h \ge 0$  (a) and  $N_h > 8$  (b) in oxygen-emulsion collisions at 3.7A GeV (open circles) and 200A GeV (solid circles).

The negative correlation between  $N_i$  and  $Q$  is determined by the nuclear geometry. For a given projectile and target,  $N_i$  increases with decreasing the impact parameter. (For  $N_b$ , there is

a saturation effect appearing if the impact parameter is small enough, i.e.  $N_b$  does not decrease.) But the projectile spectator (i.e., the value of  $Q$ ) decreases with decreasing the impact parameter. Therefore, there is a negative correlation between the multiplicity and the bound system charge.

## V. Correlations between target fragments

The correlations between  $N_b$  and  $N_h$  (a), as well as  $N_g$  and  $N_h$  (b), for oxygen-emulsion collisions at 3.7A GeV (open circles) and 200A GeV (solid circles) are given in Fig. 6. From Fig. 6 one can see that the value of  $\langle N_b \rangle$  increases with increasing  $N_h$  in the region of  $N_h \cdot 25$ , and does not depend on  $N_h$  in the region of  $N_h > 25$ . The value of  $N_b$  has a saturation effect. For the grey fragments, the value of  $\langle N_g \rangle$  increases with increasing  $N_h$ .

Figure 7(a) presents the dependence of  $\langle N_b \rangle$  on  $N_g$  for oxygen-emulsion collisions at 3.7A GeV (open circles) and 200A GeV (solid circles). One can see that the value of  $\langle N_b \rangle$  increase with increasing  $N_g$  in the region of  $N_g \cdot 8$ , and the saturation effect appears in the region of  $N_g > 8$ . The saturation effect was also observed in proton-emulsion collisions at high energy [9]. In order to study the saturation effect in detail, Fig. 7(b) presents the correlations between  $\langle N_b \rangle$  and  $N_g$  for the events with  $N_h > 8$ . One can see that the value of  $\langle N_b \rangle$  does not depend on  $N_g$ , the experimental data are the same as those in Fig. 7(a) for the events with  $N_g > 8$ . This indicates that the saturation effect is a characteristic of heavy target fragmentation in nonperipheral collisions. The mean saturation value ( $\langle N_b \rangle$ ) in Fig. 7(b) for the 3.7A and 200A GeV oxygen-emulsion collisions are  $9.5 \pm 0.3$  and  $9.3 \pm 0.3$ , respectively.

The target black fragments have a saturation effect, and the grey fragments do not. The reason is that the black fragments are the results of the target spectator's evaporation, and the grey fragments are the results of cascading collisions in the target spectator and participant.

## VI. Conclusions and discussions

To conclude, the target fragment multiplicity distribution approximately does not depend on the incident energy in the energy range from 3.7A to 200A GeV. The similarities and differences in the target fragment multiplicities at the above two energies can be explained by the nuclear geometry characteristic and the nuclear stopping effect. There is a negative correlation between the target fragment multiplicity and the bound system charge. This negative correlation is determined by the nuclear geometry. There is a saturation effect in the target black fragment multiplicity. This saturation effect is a characteristic of heavy target fragmentation in nonperipheral collisions.

Nuclear fragmentation is an important experimental phenomenon in high energy nucleus-nucleus collisions. Nuclear emulsions have been used as a target and a detector in the study of high energy collisions. We have studied the nuclear fragmentation in the energy range from the Dubna energy to the SPS energy in our previous work [10-13], and used the experimental data of nuclear emulsions elsewhere, too [14-16]. In our opinion, in the study of nuclear fragmentation, the Dubna energy region is more important than the SPS energy region, because the nuclear limiting fragmentation may set in at the Dubna energy region.

It is believed that the nuclear limiting fragmentation should apply in a definite energy range. The Dubna energy may be the initial energy of the nuclear limiting fragmentation. But we do not think the SPS energy to be the highest energy of the nuclear limiting fragmentation. We hope to compare the present results with the experimental data of nuclear fragmentation at the Relativistic

Heavy Ion Collider (RHIC) energies soon.

### Acknowledgment

The author would like to thank Profs. H. Sun and P. Zheng for supplying the emulsion sample. This work was partly finished at the Laboratory of High Energies, Joint Institute for Nuclear Research, Dubna, Russia, and the Cyclotron Institute, Texas A&M University, College Station, USA. This work was supported by the China Scholarship Council, Shanxi Provincial Foundation for Returned Overseas Scholars, Shanxi Provincial Foundation for Leading Specialists in Science, Shanxi Provincial Science Foundation for Young Specialists, and Shanxi Provincial Foundation for Key Subjects.

### References

<sup>a</sup>Electronic address: liufh@dns.sxtu.edu.cn

- [ 1 ] R. J. Glauber, in *Lectures of Theoretical Physics*, eds. W. E. Brittin and L. G. Dugam (Interscience, New York 1959), Vol. 1, p. 315.
- [ 2 ] P. L. Jain and M. M. Aggarwal, *Phys. Rev. C* **33**, 1790 (1986).
- [ 3 ] M. El-Nadi, N. Ali-Mossa, and A. Abdelsalam, *Nuovo Cimento A* **110**, 1255 (1997).
- [ 4 ] P. L. Jain, M. M. Aggarwal, and K. L. Gomber, *Phys. Rev. C* **34**, 726 (1986).
- [ 5 ] D. Ghosh, S. K. Das, and K. Ghosh, *Nuovo Cimento A* **110**, 565 (1997).
- [ 6 ] P. L. Jain, G. Singh, and A. Mukhopadhyay, *Phys. Rev. C* **50**, 1085 (1994).
- [ 7 ] G. Singh and P. L. Jain, *Phys. Rev. C* **49**, 3320 (1994).
- [ 8 ] G. Singh and P. L. Jain, *Phys. Rev. C* **54**, 3185 (1996).
- [ 9 ] A. Abduzhamilov et al., *Z. Phys. C* **40**, 223 (1988).
- [10] F. H. Liu, *Chin. J. Phys.* **38**, 1063 (2000).
- [11] F. H. Liu, *Chin. J. Phys.* **39**, 401 (2001).
- [12] F. H. Liu, *Phys. Rev. C* **59**, 941 (1999).
- [13] F. H. Liu, *Phys. Rev. C* **62**, 024613 (2000).
- [14] F. H. Liu, *Chin. J. Phys.* **39**, 243 (2001).
- [15] F. H. Liu, *Chin. J. Phys.* **39**, 248 (2001).
- [16] F. H. Liu, *Phys. Rev. D* **63**, 032001 (2001).